Journal of Radioanalytical and Nuclear Chemistry (2018) 317:1243–1252
https://doi.org/10.1007/s10967-018-6013-z

Radioiodinated doxorubicin as a new tumor imaging model: preparation, biological evaluation, docking and molecular dynamics

A. B. Ibrahim[1] · M. Alaraby Salem[2] · T. W. Fasih[3] · Alex Brown[4] · Tamer M. Sakr[2,3]

Received: 22 March 2018 / Published online: 17 July 2018

Abstract

Non-invasive molecular imaging techniques are accruing more interest in the last decades. Several radiolabelling elements have been FDA-approved and are currently used to characterize tumors. In this study, the DNA intercalating agent doxorubicin was radiolabelled with ^{125}I. Several parameters for the radiolabelling reaction were investigated and optimized. A maximum yield of 94 ± 0.3% was reached after reacting 20 µg of doxorubicin with 200 µg Chloramine-T at pH 5 for 30 min. The in vivo stability of ^{125}I-doxorubicin is validated by the low propensity for thyroid uptake in mice. The preclinical T/NT ratio was approximately 6.4 at 30 min. Docking and molecular dynamics confirmed that the radiolabelling of doxorubicin did not affect (or slightly improved its binding to DNA). Overall, ^{125}I-doxorubicin was demonstrated to be a promising non-invasive probe for solid tumor imaging.

Electronic supplementary material The online version of this article (https://doi.org/10.1007/s10967-018-6013-z) contains supplementary material, which is available to authorized users.

✉ M. Alaraby Salem
msalem@ualberta.ca

✉ Tamer M. Sakr
Tamer_sakr78@yahoo.com

[1] Labeled Compounds Department, Hot Labs Center, Atomic Energy Authority, Cairo 13759, Egypt

[2] Pharmaceutical Chemistry Department, Faculty of Pharmacy, October University of Modern Sciences and Arts (MSA), Giza, Egypt

[3] Radioactive Isotopes and Generators Department, Hot Laboratories Centre, Atomic Energy Authority, Cairo 13759, Egypt

[4] Department of Chemistry, University of Alberta, Edmonton, Canada

Graphical Abstract

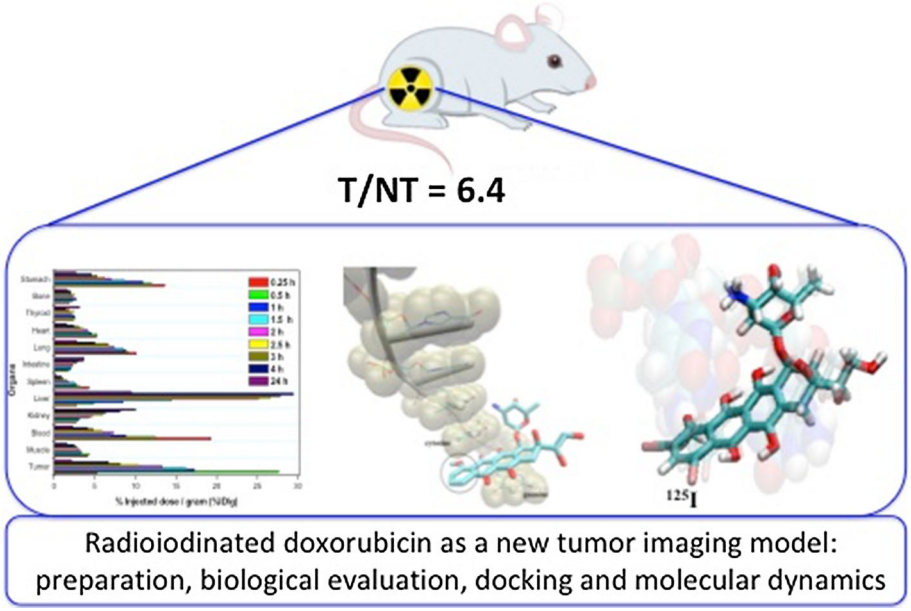

Keywords Doxorubicin · Radioidination · Tumor imaging · Molecular dynamics · Molecular docking

Introduction

Medical imaging has evolved in the last decades to be an important tool in cancer visualization and characterization [1]. Imaging at the molecular level is getting more interest due to advantages it offers as compared to conventional anatomical imaging techniques like computed x-ray tomography and magnetic resonance imaging [2]. With molecular imaging, the expression and activity of some important macromolecules involved in protein progression, like kinases and proteases, can be efficiently monitored [3]. In addition, certain key biological processes including apoptosis and angiogenesis can be traced to study cancer progression. Molecular imaging techniques also allow for the early detection of cancer and increase the associated survival rate [4]. Several techniques serve this purpose of early detection, including fluorescent-based imaging probes [5–7] and magnetic nanoparticles [8]. Single photon emission computed tomography (SPECT) and positron emission tomography (PET) imaging are FDA-approved techniques that expand the molecular imaging toolbox [9].

Radiolabelling elements include ^{99m}Tc, [10–14] ^{18}F, [15, 16] and ^{123}I [17, 18]. [^{18}F]fluorodeoxyglucose (FDG) is a widely used PET agent that has been approved for staging of many cancers [9, 19, 20]. Its selectivity stems from its resemblance to glucose, which is naturally consumed at higher rates by cancer cells [19]. However, the short half life ($t_{1/2}$ = 1.83 h) and high cost of ^{18}F limit its wide clinical application. The ability of ^{18}FDG to differentiate between a tumor and inflammation represents its main drawback as a tumor staging agent [21, 22]. Besides, ^{18}FDG can give false positive results as it showed high uptake in human and experimental inflammatory lesions [23–30]. In the last few decades, scientists investigated many radiopharmaceuticals based on radioiodine ($^{123/131}$I) or ^{99m}Tc as new models of tumor imaging-agents. Many new tumor imaging agents were evaluated in the last decade for their ability to target tumors selectively including agents such as radioiodinated anastrozole, radioiodinated epirubicin, ^{99m}Tc-meropenem, ^{99m}Tc-sunitinib, ^{99m}Tc-PyDA, ^{99m}Tc-BnAO-NI, [^{99m}Tc(CO)$_3$(IDA–PEG3–CB)]$^-$, ^{99m}Tc(CO)$_3$–labeled chlorambucil analog, ^{99m}Tc-nitridepyrazolo[1,5-a]pyrimidine, ^{99m}Tc-DETA, ^{99m}Tc-TETA, ^{99m}Tc-TEPA, ^{99m}Tc-citro-folate and ^{99m}Tc-gemcitabine [3, 10, 12, 13, 31–42]. ^{125}I has a desirable half-life time ($t_{1/2}$ = 59.4 days) and can be used as high specific activity iodide without adding carrier iodine.

Doxorubicin, Fig. 1, has been approved as a chemotherapeutic agent since the 1970s. It has a broad spectrum of activity against various malignancies, including non-Hodgkin's lymphoma, breast carcinoma, Kaposi

sarcoma, and acute lymphocytic leukemia. It is also available in pegylated forms, liposomes and frequently loaded on nano-particles [43–49]. Its mechanism of action involves intercalation between DNA bases and inhibition of the topoisomerase II enzyme [43–46]. As evident in crystal structures, the planar portion of doxorubicin intercalates between two DNA bases while further interactions (mainly H-bonds) between the six-membered daunosamine sugar and neighbouring DNA bases serve to stabilize the complex [47, 48]. The interest of using doxorubicin in imaging was based on its fluorescent properties. Recently, imaging of doxorubicin with multiphoton fluorescence techniques has been reported. [49] In addition to its innate fluorescence, the use of radiolabeled doxorubicin as a radiotracer has been previously investigated, as with ^{57}Ni-doxorubicin, [50] and ^{99m}Tc-doxorubicin. [51, 52].

We hereby describe the synthesis of ^{125}I-doxorubicin and evaluated it as a new tumor-imaging model. The suggested structures are further studied on the molecular level using docking and molecular dynamics. While molecular docking can shed light on the possible poses for the interaction between the drug (doxorubicin derivatives) and the target (DNA), molecular dynamics (MD) can offer a more realistic simulation of the interaction dynamics over a trajectory [53]. With MD, the stability of the drug-DNA complex can be determined while factoring in the effect of explicit solvent molecules [53]. In addition, the affinity score is calculated in MD as a time-averaged property. The affinity scores from both in silico techniques are compared and discussed.

Experimental

Materials and equipment

All chemicals were of analytical grade. Doxorubicin [$C_{27}H_{29}NO_{11}$], M.wt. = 543.52 g/mol, and all other chemicals, Sigma-Aldrich Company, Egypt. No-carrier-added sodium iodide (NCA Na^{125}I, 3.7 GBq/mL), Radioisotope Production Factory, Atomic Energy Authority, Egypt. Whatman paper no. 1, Merck, Germany. A NaI(Tl) γ-ray scintillation counter, Scaler Ratemeter SR7 model, UK. Shimadzu HPLC, UV spectrophotometer detector SpD-6A, Reversed phase Waters Symmetry C18 (RP-18) column, Lischrosorb, Merck, pump LC-9A, fraction Collector-LKB, Bromma, Japan.

Animal model

Normal Swiss albino mice (20–40 g) were obtained from Helwan University, Egypt. Animal studies were conducted according to the Egyptian Atomic Energy Authority (EAEA) guidelines that approved by the animal ethics committee were followed for all animal studies.

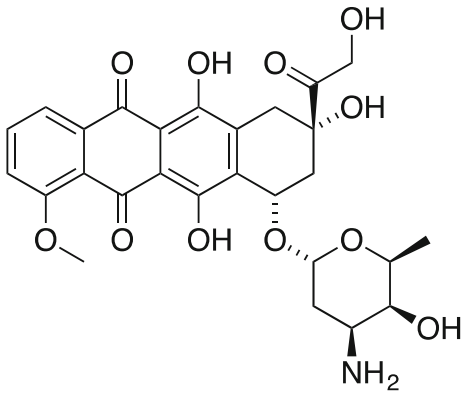

Fig. 1 Doxorubicin

Radioiodination procedure

Synthesis of radioiodinated doxorubicin was carried out by direct electrophilic substitution with ^{125}I using chloramine-T (CAT) as an oxidizing agent. In addition to its desirable half-life time ($t_{1/2}$ = 59.4 days), ^{125}I affords the ability to use high specific activity iodide no carried added iodine [54–57]. Various reaction parameters, including the chloramine-T amount, doxorubicin amount, reaction pH and reaction time, were optimized to obtain the maximum radiochemical yield. Doxorubicin, CAT, and sodium metabisulfite stock solutions were prepared with concentrations of 0.4, 1.0 and 10.0 mg/mL, respectively. In amber colored vials, the different volumes containing (4–160 μg) of doxorubicin were mixed with different volumes (50–350 μL) of freshly prepared CAT solution containing (50–350 μg) of CAT. 10 μL of ^{125}I (7.2 MBq) was added to each of the reaction mixtures and then the pH was adjusted by 0.1 N HCl and 0.1 N NaOH to be in the range of 3–12. Each reaction mixture was completed to 0.5 mL by distilled water and shaken by electric vortex. The reaction time (5–90 min) was studied. 50 μL sodium metabisulfite solution (10 mg/mL) was used to quench the reaction by reducing excess iodine (I_2) to iodide (I^-) [54–57].

Quality control of radioiodinated doxorubicin

Radiochemical yield and in vitro assay assessment

Ascending paper chromatography (PC) was used to assess the radiochemical yield and in vitro stability of ^{125}I-doxorubicin. In the paper chromatography (PC) method, Whatman paper number 1 strips were developed using a fresh mixture of 70% v/v methanol as a developing solvent. Free radioiodide (I^-) stayed at the spotting point (R_f = 0–0.1), while the radioiodinated doxorubicin reached R_f = 0.85. On each paper srtip (1 cm × 13 cm), 1–2 μL of the prepared kit was seeded 2 cm above the lower edge,

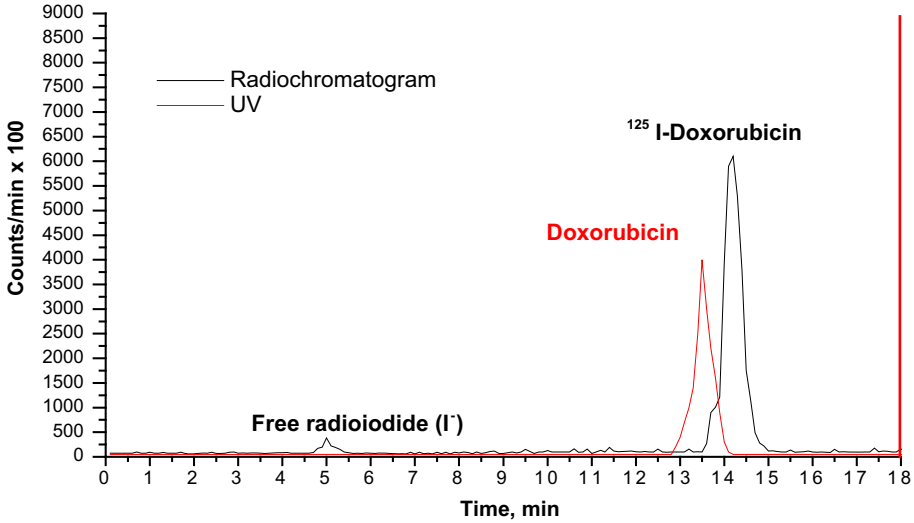

Fig. 2 HPLC-Radiochromatogram of radioiodinated doxorubicin

evaporated, and then developed. After full development, each strip was dried and cut into strips (1 cm) then counted in a well type γ-counter.

Purification and radiochemical purity assessment

For purification and radiochemical purity evaluation of radioiodinated doxorubicin, HPLC was used. An optimum reaction mixture (500 μL) was fed into a Lichrospher RP18 column. The HPLC was operated at 254 nm wavelength using acetonitrile: water (15:85, v/v) with 1 mL/min flow rate. Each 0.5 mL fraction was collected using a fraction collector and counted in a well type γ-counter. As shown in Fig. 2, the retention time of free radioiodide and radioiodinated doxorubicin were at 5 and 14.3 min, respectively. Collecting fractions from 13.5 to 15 min provided the purified radioiodinated doxorubicin.

Solid tumor induction in mice

Ehrlich ascites carcinoma (EAC) derived from a murine mammary carcinoma was used to induce solid tumor. The parent tumor line EAC was diluted with sterile physiological solution. For inducing a solid tumor, 200 μL of EAC solution was injected intramuscularly in the right thigh of female Albino mice and left to grow for 4–6 days [31, 57, 58].

Biodistribution study of radioiodinated doxorubicin

Radioiodinated doxorubicin biodistribution in tumor bearing female Albino Swiss mice was evaluated out at 20 min, 0.5, 1, 1.5, 2, 2.5, 3, 4, and 24 h post-injection (p.i.). Radioiodinated doxorubicin (3.7 MBq) in 10 μL was intravenously injected into the mouse-tail vein. Then each mouse was anesthetized and weighed. Samples of fresh blood, bone, and muscle were separated and counted in a well type γ-counter and they were calculated to be 7, 10, and 40% of the total body weight, respectively [58–60]. All other body organs and tissues were separated and counted in a well type γ-counter. Percent-injected dose per gram (% ID/g ± SEM) in a population of five mice for each time point are reported.

Statistical analysis

One-way analysis of variance test evaluated all data. Results for p are reported, and all the results are given as mean ± SEM. The level of significance was set at $p < 0.05$.

Molecular docking

Docking was performed with Autodock4 [61]. The input files were prepared using Autodock Tools [61]. The crystal structure (PDF ID: 1d12) [47] used for the DNA and the intercalating doxorubicin has a resolution of 1.7 Å and an R-value of 0.177. The crystal is composed of a single-stranded DNA with a total 6 of DNA bases where doxorubicin is between the fifth cytosine and the sixth guanine. All extra ligands other than doxorubicin were removed. Gasteiger charges were used to assign partial charges for the DNA and all ligands. In total, four ligands were docked: doxorubicin (ligand 1), 1-iodotetracene (ligand 2), 3-iodotetracene (ligand 3), and 1,3-diiodotetracene (ligand 4) doxorubicin derivatives. All ligands are illustrated in Fig. 8. Rigid-rigid docking was adopted; that is, all rotatable bonds of the ligands were fixed at their crystallographic values. We docked the ligands using a genetic algorithm (50 steps) in a box centered on the native ligand with default Autodock parameters. Cluster analysis was

done and the reported values are for the highest populated clusters.

Molecular dynamics

Four dynamics trajectories were run for the DNA in complex with the four ligands given in Fig. 8, one at a time. Each of the four trajectories started from the crystallographic coordinates (PDB ID: 1d12). Ambertools 14 [62] was used to prepare initial topology and coordinate files for the complexes. The PDB file (PDB ID 1d12) was cleaned from other ligands except doxorubicin while retaining crystallographic water molecules. The structures for protein–ligand complexes were then prepared using the pdb4amber and reduce programs [63]. The forcefield AMBER ff12SB [64, 65], which is suitable for both DNA and proteins, was used to parameterize the DNA residues. On the other hand, doxorubicin (ligand 1) and other ligands (ligands 2–4) were parameterized using ANTECHAMBER [66] to generate parameters that are consistent with the General Amber Force Field (GAFF) [66]. The semi-empirical method AM1-BCC was used to assign charges. The complex was solvated using an extra 2608 TIP3P water

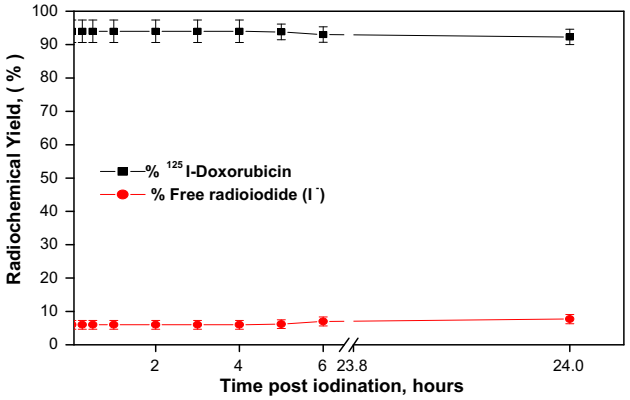

Fig. 4 In vitro stability of radioiodinated doxorubicin

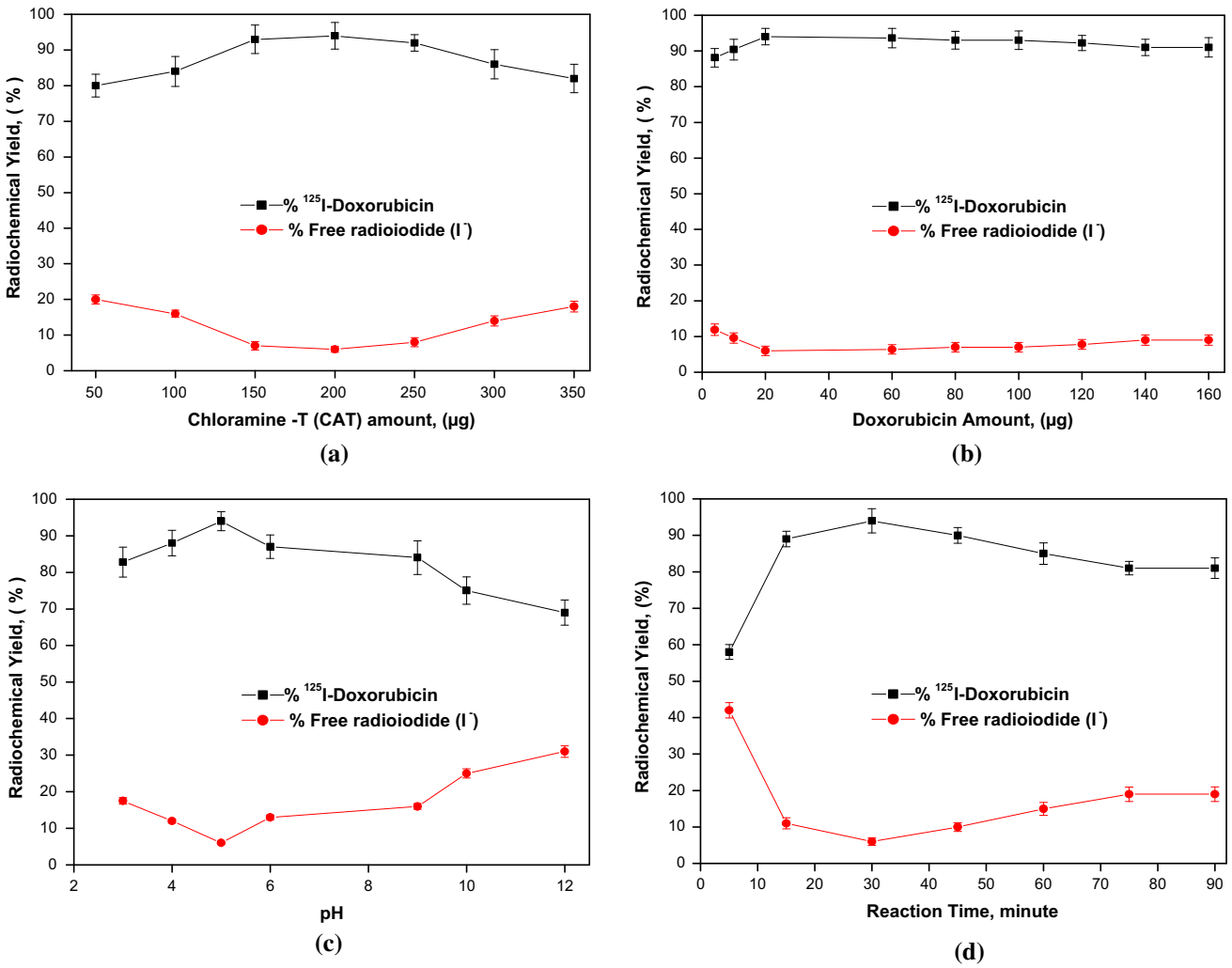

Fig. 3 Effect of different parameters on the radiochemical yield of radioiodinated doxorubicin

molecules in an octahedral box with the addition of four sodium ions to neutralize the negatively-charged DNA fragment. Using the AMBER Molecular Dynamics package [62], we adopted a standard protocol for molecular dynamics consisting of minimization, heating, density equilibration, and production. The AMBER input files are similar to those in the supplementary information of the previous work of Salem and Brown [67]. The trajectory lengths for heating, density equilibration, and production were 20 ps, 50 ps and 10 ns, respectively. The trajectories were analyzed using CPPTraj [68], XMgrace [69], and VMD [70].Free energy calculations were done using the Generalized Born-Surface Area (GBSA) algorithm implemented in AMBER12 [71].

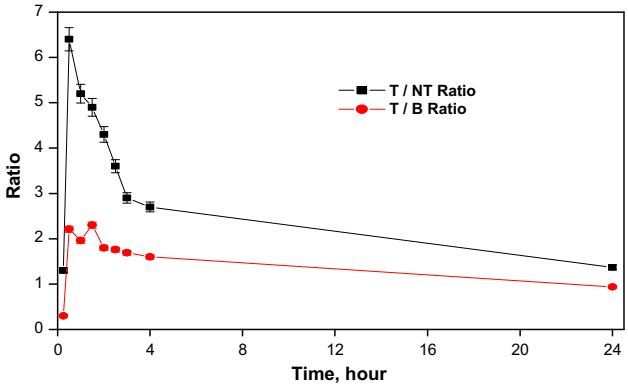

Fig. 6 Tumor/normal muscle (T/NT) and tumor/blood (T/B) ratios of radioiodinated doxorubicin

Results and discussion

Radioiodination

Radioiodination of doxorubicin was optimized through studying chloramine-T (CAT) amount, doxorubicin amount, pH and reaction time parameters to obtain the maximum radiochemical yield [54–57]. A maximum radiochemical purity (94 ± 0.3%) was obtained using 200 µg of CAT amount, 20 µg doxorubicin amount, at pH 5 and for 30 min reaction time Fig. 3.

In vitro stability of radioiodinated doxorubicin

To determine the suitable time for radioiodinated doxorubicin injection to avoid undesired radioactive products formation, the in vitro stability was studied. Radioiodinated doxorubicin was in vitro stable up to 24 h as shown in Fig. 4.

Biodistribution study of radioiodinated doxorubicin

The distribution of radioiodinated doxorubicin was studied in solid tumor-bearing mice, percent injected dose per gram (%ID/g) at 20 min, 0.5, 1, 1.5, 2, 2.5, 3, 4 and 24 h post-injection (p.i.). The %ID/g of radioiodinated doxorubicin in different body organs and fluids is illustrated in Fig. 5. Radioiodinated doxorubicin did not show selective accumulation in a specific body organ, besides it was eliminated via hepatobiliary pathway. The low thyroid uptakes of radioiodinated doxorubicin confirm their in vivo stability. The tumor tissue (mouse right leg muscle)/normal tissue (mouse left leg muscle) (T/NT) ratio is the main parameter to evaluate the selectivity and sensitivity of radioiodinated doxorubicin to solid tumor [3, 13, 14].

Figure 6 shows the radioiodinated doxorubicin Tumor/Normal muscle (T/NT) ratio in solid tumor-bearing mice.

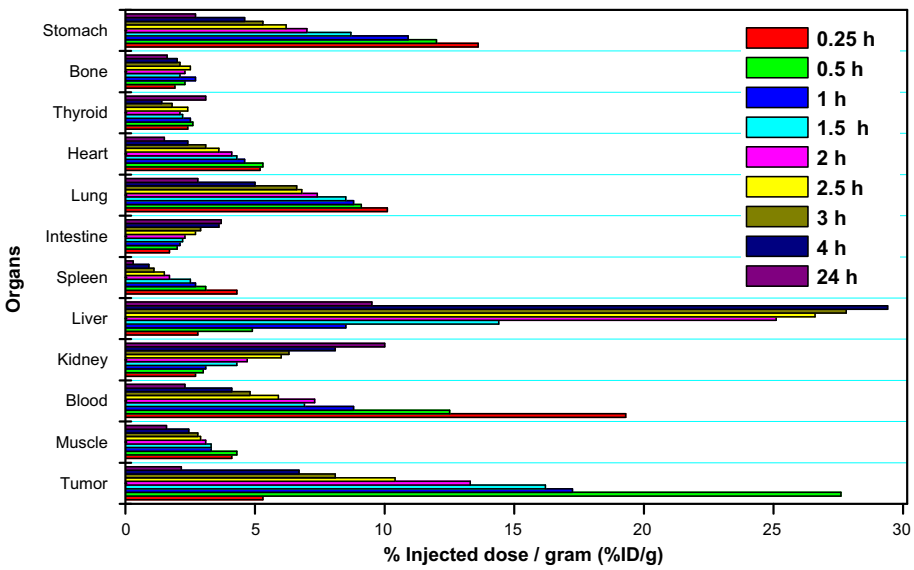

Fig. 5 Biodistribution study of radioiodinated doxorubicin

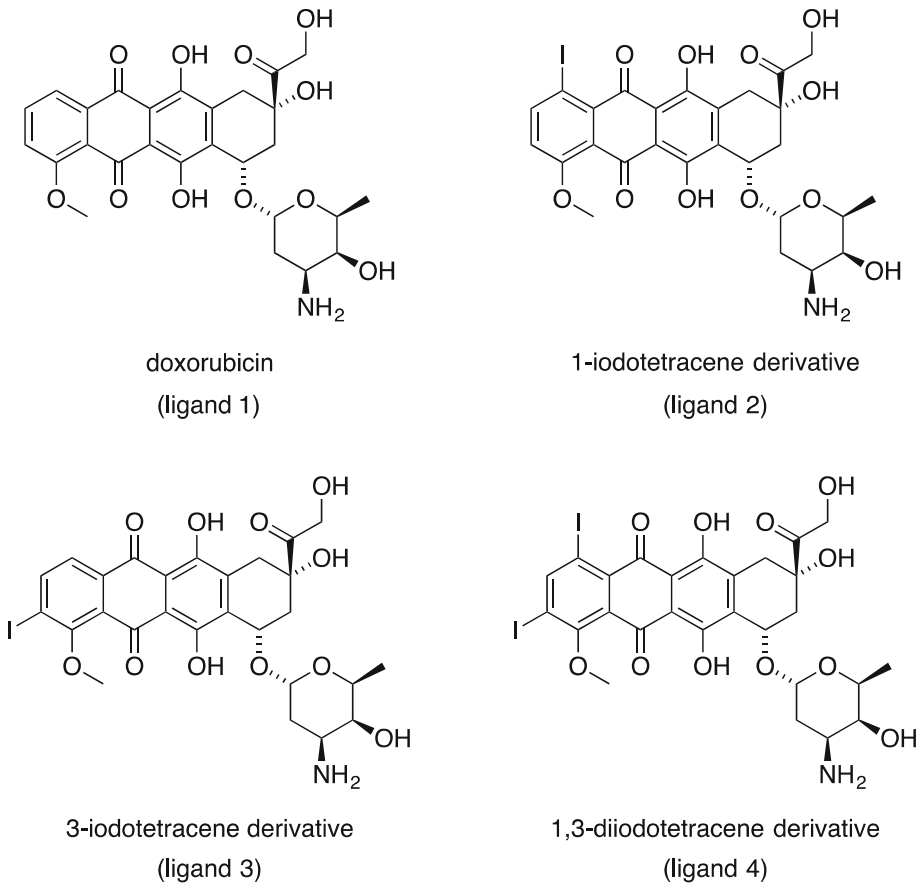

Fig. 7 The ligands included in the docking and MD simulation studies

Table 1 Numerical results for the docking and MD experiments

Ligand	Docking		MD
	Dock score (kcal/mol)	vDW, H-bond and desolvation energy (kcal/mol)	GBSA energy (kcal/mol)
Native	− 7.1	− 9.4	− 15.2
Para	− 7.1	− 9.3	− 16.6
Ortho	− 7.1	− 9.5	− 18.1
Ortho–para	− 7.4	− 9.6	− 18.9

T/NT ratio was ~ 1.4 at 15 min p.i. that increased to its maximum value of ~ 6.4 at 30 min p.i. confirming high tumor cells selectivity. This high preclinical T/NT ratio presents radioiodinated doxorubicin as a new non-invasive solid tumor imaging probe if compared other different agents such as: $[^{99m}Tc(CO)_3(IDA–PEG3–CB)]^-$ (3.45, 3 h p.i.), ^{99m}Tc-BnAO-NI (2.59, 2 h p.i.), $^{99m}Tc(CO)_3$–labeled chlorambucil analog (3.2 at 3 h p.i), radioiodinated epirubicin (5.2 ± 0.09 at 1 h p.i.), ^{99m}Tc-nitridepyrazolo[1,5-a]pyrimidine (2.2 at 1 h p.i.), radioiodinated anastrozole (4.7 ± 0.06 at 2 h p.i.), ^{99m}Tc-DETA (2.47 at 4 h p.i.), ^{99m}Tc-PyDA (3 at 1 h p.i.), ^{99m}Tc-TETA (2.45 at 4 h p.i.), ^{99m}Tc-sunitinib (3 at 1 h p.i.), ^{99m}Tc-TEPA (2.91 at 4 h p.i.), ^{99m}Tc-meropenem (3.5 at 1 h p.i.), ^{99m}Tc-citro-folate (4.3 at 4 h p.i.), and ^{99m}Tc-gemcitabine (4.9 at 2 h p.i.) [3, 10, 12–14, 32–42]. All of these results present radioiodinated doxorubicin as a promising solid tumor-imaging agent.

Molecular docking

The ligands used in the docking experiment are illustrated in Fig. 7. As shown in Table 1, the iodo-substituted doxorubicins have similar predicted binding affinity relative to the native ligand. Figure 8 shows the bioactive binding pose of doxorubicin, as given in the crystal structure (PDB ID: 1d12). Any substitution on the highlighted ring in Fig. 8 will cause the iodine to be more exposed to the

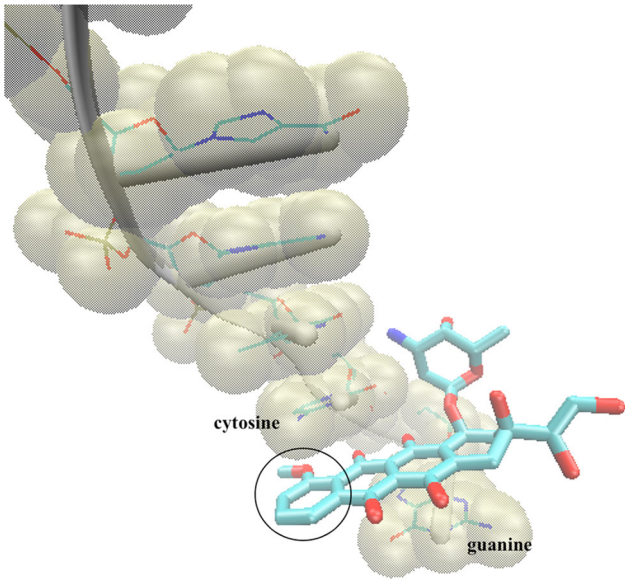

Fig. 8 The binding pose of doxorubicin as given in the crystal structure (PDB ID: 1d12). The image was generated using VMD

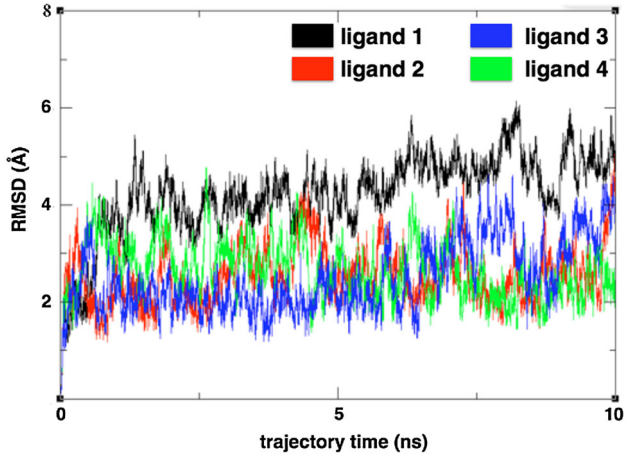

Fig. 9 RMSD fluctuation over a 10 ns MD trajectory for the 4 ligands (see Fig. 9) using the 1d12 crystal structure

solvent. Since iodine is of significantly greater polarizability than hydrogen, it is capable of forming favorable London dispersion forces with water in the surrounding medium. Hence, iodo-substitution of doxorubicin is accompanied by less solvation penalty.

This hypothesis is supported by the values reported for the term for van der Waals (and hence London dispersion forces), H-bond, and desolvation energies in Table 1. The docking scores shows marginal improvement (slightly more negative) energy for the diiodo-substituted ligand. The energy difference of 0.3 kcal/mol is not enough to draw a conclusion on the relative affinities and thus molecular dynamics was performed to have a more accurate picture.

Molecular dynamics (MD)

The stability and binding affinity of the four ligands in complex with the DNA fragment were further studied via MD. Figure 9 shows the root-mean-square deviations (RMSD) over a trajectory of 10 ns. It is clear from Fig. 9 that the iodo-substituted ligands have better stability (lower RMSD average) than the native doxorubicin. The generally high RMSD fluctuations can be rationalized by the simulation conditions where the ligand is sandwiched between the last two DNA bases in the DNA fragment, see Fig. 7. This allowed more flexibility for the terminal guanine base. Table 1 shows the results for binding affinity of each ligand using GBSA algorithm over the interval of 10 ns starting from the beginning of the simulation. Similar to the docking studies, the iodo-substituted doxorubicin has better predicted binding affinity. Interestingly, the ligand with both ortho and para substitutions with respect to the 4-methoxy substituent (ligand 4) has the best binding affinity in the MD study which is in agreement with the rigid docking study.

Conclusion

In this work, we present the synthesis of ^{125}I-doxorubicin together with its evaluation as a promising solid tumor-imaging agent. The in vitro and in vivo stability of ^{125}I-doxorubicin were confirmed. In addition, the preclinical T/NT ratio was large ($\sim$ 6.4 at 30 min) as compared to similar agents. Docking studies showed equivalent binding affinities for free doxorubicin and the iodinated models. Studying the molecular dynamics trajectories for doxorubicin and three suggested models of ^{125}I-doxorubicin reveal better stability and slightly higher affinity for the DNA-^{125}I-doxorubicin complex. Overall, radioiodinated doxorubicin appears to be a promising non-invasive probe for solid tumor imaging.

Acknowledgements This research was enabled in part by support provided by Westgrid (www.westgrid.ca) and Compute/Calcul Canada (www.computecanada.ca).

Compliance with ethical standards

Conflict of interest All authors declared no conflict of interest.

Ethical approval Authors report that all applicable international and institutional guidelines for the care and use of animals were followed.

References

1. Weissleder R (2006) Molecular imaging in cancer. Science 312:1168–1171
2. Saha GB (2012) Physics and radiobiology of nuclear medicine. Springer, New York
3. Sakr TM, El-Safoury DM, Awad GAS, Motaleb MA (2013) Biodistribution of ^{99m}Tc-sunitinib as a potential radiotracer for tumor hypoxia imaging. J Label Compd Radiopharm 56:392–395
4. Etzioni R, Urban N, Ramsey S et al (2003) Early detection: the case for early detection. Nat Rev Cancer 3:243
5. Marten K, Bremer C, Khazaie K, Sameni M, Sloane B, Tung CH, Weissleder R (2002) Detection of dysplastic intestinal adenomas using enzyme-sensing molecular beacons in mice. Gastroenterology 122:406–414
6. Alencar H, Mahmood U, Kawano Y, Hirata T, Weissleder R (2005) Novel multiwavelength microscopic scanner for mouse imaging. Neoplasia 7:977–983
7. Evans JA, Nishioka NS (2005) Endoscopic confocal microscopy. Curr Opin Gastroenterol 21:578–584
8. Harisinghani MG, Barentsz J, Hahn PF, Deserno W, Tabatabaei S, van de Kaa CH, de la Rosette J, Weissleder R (2003) Non-invasive detection of clinically occult lymph-node metastases in prostate cancer. N Engl J Med 348:2491–2499
9. Juweid ME, Cheson BD (2006) Positron-emission tomography and assessment of cancer therapy. N Engl J Med 354:496–507
10. Altiparmak B, Lambrecht FY, Bayrak E, Durkan K (2010) Design and synthesis of ^{99m}Tc-citro-folate for use as a tumor-targeted radiopharmaceutical. Int J Pharm 400:8–14
11. Santos-Cuevas CL, Ferro-Flores G, de Murphy CA, Ramírez FDM, Luna- Gutiérrez MA, Pedraza-López M, García-Becerra R, Ordaz-Rosado D (2009) Design, preparation, in vitro and in vivo evaluation of ^{99m}Tc-N_2S_2-Tat (49-57)-bombesin: a target-specific hybrid radiopharmaceutical. Int J Pharm 375:75–83
12. de Barros ALB, das Graças Mota L, de Aguiar Ferreira C, de Oliveira MC, de Góes AM, Cardoso VN (2010) Bombesin derivative radiolabeled with technetium-99m as agent for tumor identification. Bioorg Med Chem Lett 20:6182–6184
13. Sakr TM, Motaleb MA, Ibrahim IT (2012) ^{99m}Tc-meropenem as a potential SPECT imaging probe for tumor hypoxia. J Radioanal Nucl Chem 291:705–710
14. Sakr TM, Essa BM, El-Essawy FA, El-Mohty AA (2014) Synthesis and biodistribution of ^{99m}Tc-PyDA as a potential marker for tumor hypoxia imaging. Radiochemistry 56:76–80
15. Rasey JS, Koh WJ, Evans ML, Peterson LM, Lewellen TK, Graham MM, Krohn KA (1996) Quantifying regional hypoxia in human tumors with positron emission tomography of [^{18}F] fluoromisonidazole: a pretherapy study of 37 patients. Int J Radiat Oncol Biol Phys 36:417–428
16. Rischin D, Hicks RJ, Fisher R, Binns D, Corry J, Porceddu S, Peters LJ (2006) Prognostic significance of [^{18}F]-misonidazole positron emission tomography-detected tumor hypoxia in patients with advanced head and neck cancer randomly assigned to chemoradiation with or without tirapazamine: a substudy of Trans-Tasman Radiation Oncolo. J Clin Oncol 24:2098–2104
17. Parliament MB, Chapman JD, Urtasun RC, McEwan AJ, Golberg L, Mercer JR, Mannan RH, Wiebe LI (1992) Non-invasive assessment of human tumour hypoxia with ^{123}I-iodoazomycin arabinoside: preliminary report of a clinical study. Br J Cancer 65:90
18. Stypinski D, McQuarrie SA, McEwan AJB, Wiebe LI (2018) Pharmacokinetics and scintigraphic imaging of the hypoxia-imaging agent [^{123}I] IAZA in healthy adults following exercise-based cardiac stress. Pharmaceutics 10:25
19. Quon A, Gambhir SS (2005) FDG-PET and beyond: molecular breast cancer imaging. J Clin Oncol 23:1664–1673
20. Guller U, Nitzsche EU, Schirp U, Viehl CT, Torhorst J, Moch H, Langer I, Marti WR, Oertli D, Harder F, Zuber M (2002) Selective axillary surgery in breast cancer patients based on positron emission tomography with ^{18}F-fluoro-2-deoxy-D-glucose: not yet! Breast Cancer Res Treat 71:171–173
21. Larson SM (1994) Cancer or inflammation? A holy grail for nuclear medicine. J Nucl Med 35:1653–1655
22. Stöber B, Tanase U, Herz M et al (2006) Differentiation of tumour and inflammation: characterisation of [methyl-3 H] methionine (MET) and O-(2-[^{18}F] fluoroethyl)-L-tyrosine (FET) uptake in human tumour and inflammatory cells. Eur J Nucl Med Mol Imaging 33:932–939
23. Kubota R, Yamada S, Kubota K, Ishiwata K, Tamahashi N (1992) Intratumoral distribution of fluorine-18-fluorodeoxyglucose in vivo: high accumulation in macrophages and granulation tissues studied by microautoradiography. J Nucl Med 33:1972–1980
24. Kubota K, Kubota R, Yamada S, Tada M (1995) Effects of radiotherapy on the cellular uptake of carbon-14 labeledL-methionine in tumor tissue. Nucl Med Biol 22:193–198
25. Yamada S, Kubota K, Kubota R, Ido T, Tamahashi N (1995) High accumulation of fluorine-18-fluorodeoxyglucose in turpentine-induced inflammatory tissue. J Nucl Med 36:1301–1306
26. Kubota R, Kubota K, Yamada S, Tada M, Takahashi T, Iwata R (1995) Methionine uptake by tumor tissue: a microautoradiographic comparison with FDG. J Nucl Med 36:484–492
27. Sugawara Y, Gutowski TD, Fisher SJ, Brown RS, Wahl RL (1999) Uptake of positron emission tomography tracers in experimental bacterial infections: a comparative biodistribution study of radiolabeled FDG, thymidine, L-methionine, 67 Ga-citrate, and ^{125}I-HSA. Eur J Nucl Med 26:333–341
28. Reinhardt MJ, Kubota K, Yamada S, Iwata R, Yaegashi H (1997) Assessment of cancer recurrence in residual tumors after fractionated radiotherapy: a comparison of fluorodeoxyglucose, L-methionine and thymidine. J Nucl Med 38:280
29. Gutowski TD (1992) Experimental studies of 18-F-2-fluoro-2-deoxy-D-glucose (FDG) in infection and in reactive lymph nodes. J Nucl Med 33:925
30. Wahl RL, Fisher SJ (1993) A comparison of FDG, L-methionine and thymidine accumulation into experimental infections and reactive lymph-nodes. J Nucl Med 34:104
31. Al-Wabli RI, Sakr TM, Khedr MA, Selim AA, El MA, Zaghary WA (2016) Platelet-12 lipoxygenase targeting via a newly synthesized curcumin derivative radiolabeled with technetium-99 m. Chem Cent J 10:1–12
32. Wan WX, Yang M, Pan SR, Yu CJ, Wu NJ (2008) [^{99m} Tc]polyamine analogs as potential tumor imaging agent. Drug Dev Res 69:520–525
33. Mallia MB, Subramanian S, Mathur A et al (2010) Synthesis and evaluation of 2-, 4-, 5-substituted nitroimidazole-iminodiacetic acid-^{99m}Tc(CO)3 complexes to target hypoxic tumors. J Label Compd Radiopharm 53:535–542
34. Wang J, Yang J, Yan Z, Duan X, Tan C, Shen Y, Wu W (2011) Synthesis and preliminary biological evaluation of [^{99m}-$Tc(CO)_3$(IDA–PEG_3–CB)]$^-$ for tumor imaging. J Radioanal Nucl Chem 287:465–469
35. Ding R, He Y, Xu J, Liu H, Wang X, Feng M, Qi C, Zhang J, Peng C (2012) Preparation and bioevaluation of ^{99m}Tc nitrido radiopharmaceuticals with pyrazolo[1,5-a]pyrimidine as tumor imaging agents. Med Chem Res 21:523–530
36. Machac J, Krynyckyi B, Kim C (2002) Peptide and antibody imaging in lung cancer. Semin Nucl Med 32:276–292
37. Ibrahim AB, Sakr TM, Khoweysa OM, Motaleb MA, El-Bary AA, El-Kolaly MT (2014) Formulation and preclinical evaluation

of ^{99m}Tc-gemcitabine as a novel radiopharmaceutical for solid tumor imaging. J Radioanal Nucl Chem 302:179–186
38. Hsia CC, Huang FL, Hung GU, Shen LH, Chen CL, Wang HE (2011) The biological characterization of ^{99m}Tc-BnAO-NI as a SPECT probe for imaging hypoxia in a sarcoma-bearing mouse model. Appl Radiat Isot 69:649–655
39. Kuchar M, Oliveira MC, Gano L, Santos I, Kniess T (2012) Radioiodinated sunitinib as a potential radiotracer for imaging angiogenesis—radiosynthesis and first radiopharmacological evaluation of 5-[^{125}I]Iodo-sunitinib. Bioorg Med Chem Lett 22:2850–2855
40. Baishya R, Nayak DK, Chatterjee N, Halder KK, Karmakar S, Debnath MC (2014) Synthesis, characterization, and biological evaluation of ^{99m}Tc(CO)$_3$-labeled peptides for potential use as tumor targeted radiopharmaceuticals. Chem Biol Drug Des 83:58–70
41. Breeman WA, Hofland LJ, Bakker WH, van der Pluij M, Van Koetsveld PM, de Jong M, Setyono-Han B, Kwekkeboom DJ, Visser TJ, Lamberts SW, Krenning EP (1993) Radioiodinated somatostatin analogue RC-160: preparation, biological activity, in vivo application in rats and comparison with [123I-Tyr3]octreotide. Eur J Nucl Med 20:1089–1094
42. Maecke HR, Reubi JC (2011) Somatostatin receptors as targets for nuclear medicine imaging and radionuclide treatment. J Nucl Med 52:841–844. https://doi.org/10.2967/jnumed.110.084236
43. Tacar O, Sriamornsak P, Dass CR (2013) Doxorubicin: an update on anticancer molecular action, toxicity and novel drug delivery systems. J Pharm Pharmacol 65:157–170
44. Fornari FA, Randolph JK, Yalowich JC, Ritke MK, Gewirtz DA (1994) Interference by doxorubicin with DNA unwinding in MCF-7 breast tumor cells. Mol Pharmacol 45:649–656
45. Momparler RL, Karon M, Siegel SE, Avila F (1976) Effect of adriamycin on DNA, RNA, and protein synthesis in cell-free systems and intact cells. Cancer Res 36:2891–2895
46. Pommier Y, Leo E, Zhang H, Marchand C (2010) DNA topoisomerases and their poisoning by anticancer and antibacterial drugs. Chem Biol 17:421–433
47. Frederick CA, Williams LD, Ughetto G, Van der Marel GA, Van Boom JH, Rich A, Wang AH (1990) Structural comparison of anticancer drug-DNA complexes: adriamycin and daunomycin. Biochemistry 29:2538–2549
48. Pigram W-J, Fuller W, Hamilton LD (1972) Stereochemistry of intercalation: interaction of daunomycin with DNA. Nat New Biol 235:17
49. Carlson M, Watson AL, Anderson L, Largaespada DA, Provenzano PP (2017) Multiphoton fluorescence lifetime imaging of chemotherapy distribution in solid tumors. J Biomed Opt 22:116010
50. Zweit J, Carnochan P, Goodall R, Ott R (1994) Nickel-57-doxorubicin, a potential radiotracer for pharmacokinetic studies using PET: production and radiolabelling. J Nucl Biol Med Med (Turin, Italy 1991) 38:18–21
51. Rizvi FA, Bokhari TH, Roohi S, Mushtaq A (2012) Direct labeling of doxorubicin with technetium-99m: its optimization, characterization and quality control. J Radioanal Nucl Chem 293:303–307
52. Fernandes RS, de Oliveira Silva J, Lopes SCA, Chondrogiannis S, Rubello D, Cardoso VN, Oliveira MC, Ferreira LA, de Barros AL (2016) Technetium-99m-labeled doxorubicin as an imaging probe for murine breast tumor (4T1 cell line) identification. Nucl Med Commun 37:307–312
53. Alonso H, Bliznyuk AA, Gready JE (2006) Combining docking and molecular dynamic simulations in drug design. Med Res Rev 26:531–568
54. Swidan MM, Sakr TM, Motaleb MA et al (2014) Radioiodinated acebutolol as a new highly selective radiotracer for myocardial perfusion imaging. J Label Compd Radiopharm 57:593–599
55. Swidan MM, Sakr TM, Motaleb MA, El-Bary AA, El-Kolaly MT (2015) Preliminary assessment of radioiodinated fenoterol and reproterol as potential scintigraphic agents for lung imaging. J Radioanal Nucl Chem 303:531–539
56. Sakr TM (2014) Synthesis and preliminary affinity testing of 123I/125I-N-(3-iodophenyl)-2-methylpyrimidine-4,6-diamine as a novel potential lung scintigraphic agent. Radiochemistry 56:200–206
57. Ibrahim AB, Sakr TM, Khoweysa OM, Motaleb MA, El-Bary AA, El-Kolaly MT (2015) Radioiodinated anastrozole and epirubicin as potential targeting radiopharmaceuticals for solid tumor imaging. J Radioanal Nucl Chem 303:967–975
58. Essa BM, Sakr TM, Khedr MA, El-Essawy FA, El-Mohty AA (2015) 99mTc-amitrole as a novel selective imaging probe for solid tumor: in silico and preclinical pharmacological study. Eur J Pharm Sci 76:102–109
59. Sakr TM, Nawar MF, Fasih TW, El-Bayoumy S, El-Rehim HA (2017) Nano-technology contributions towards the development of high performance radioisotope generators: the future promise to meet the continuing clinical demand. Appl Radiat Isot 129:67–75
60. Mohamed KO, Nissan YM, El-Malah AA, Ahmed WA, Ibrahim DM, Sakr TM, Motaleb MA (2017) Design, synthesis and biological evaluation of some novel sulfonamide derivatives as apoptosis inducers. Eur J Med Chem 135:424–433
61. Morris GM, Huey R, Lindstrom W, Sanner MF, Belew RK, Goodsell DS, Olson AJ (2009) AutoDock4 and AutoDockTools4: automated docking with selective receptor flexibility. J Comput Chem 30:2785–2791
62. Case DA, Darden TA, Cheatham TE III, Simmerling CL, Wang J, Duke RE, Luo R, Walker RC, Zhang W, Merz KM, Roberts B (2012) AMBER 12. University of California, San Francisco
63. Word JM, Lovell SC, Richardson JS, Richardson DC (1999) Asparagine and glutamine: using hydrogen atom contacts in the choice of side-chain amide orientation1. J Mol Biol 285:1735–1747
64. Cornell WD, Cieplak P, Bayly CI, Gould IR, Merz KM, Ferguson DM, Spellmeyer DC, Fox T, Caldwell JW, Kollman PA (1995) A second generation force field for the simulation of proteins, nucleic acids, and organic molecules. J Am Chem Soc 117:5179–5197
65. Hornak V, Abel R, Okur A, Strockbine B, Roitberg A, Simmerling C (2006) Comparison of multiple Amber force fields and development of improved protein backbone parameters. Proteins Struct Funct Bioinform 65:712–725
66. Wang J, Wang W, Kollman PA, Case DA (2006) Automatic atom type and bond type perception in molecular mechanical calculations. J Mol Graph Model 25:247–260
67. Alaraby Salem M, Brown A (2015) Two-photon absorption of fluorescent protein chromophores incorporating non-canonical amino acids: TD-DFT screening and classical dynamics. Phys Chem Chem Phys 17:25563–25571
68. Roe DR, Cheatham TE (2013) PTRAJ and {CPPTRAJ}: software for processing and analysis of molecular dynamics trajectory data. J Chem Theory Comput 9:3084–3095
69. Turner PJ (2005) XMGRACE, Version 5.1. 19. Center for Coastal and Land-Margin Research, Oregon Graduate Institute of Science and Technology, Beaverton, OR
70. Humphrey W, Dalke A, Schulten K (1996) VMD: visual molecular dynamics. J Mol Graph 14:33–38
71. Kollman PA, Massova I, Reyes C, Kuhn B, Huo S, Chong L, Lee M, Lee T, Duan Y, Wang W, Donini O (2000) Calculating structures and free energies of complex molecules: combining molecular mechanics and continuum models. Acc Chem Res 33:889–897